

# Optical Simulation and PSF Analysis

Yuanhao Wang

October 11, 2025

## 1 Experiment

For the evaluation of the results, we consider the Thorlabs LB1761 (a simple BK7 biconvex singlet lens) and perform a simulation using an f/8 aperture placed 2 mm from the second lens surface. We map  $[R1, T, R2, D2, OD]$  (mm) as: **R1 = 24.5**, **T = 9**, **R2 = -24.5**, **D2 = 20.5**, **OD = 3.175** (f/8).

We only use **OD = 6.25 mm** for the sampling (N) sweep and off-axis experiments to better illustrate the effects of varying N and off-axis aberrations.

We conducted the following experiments:

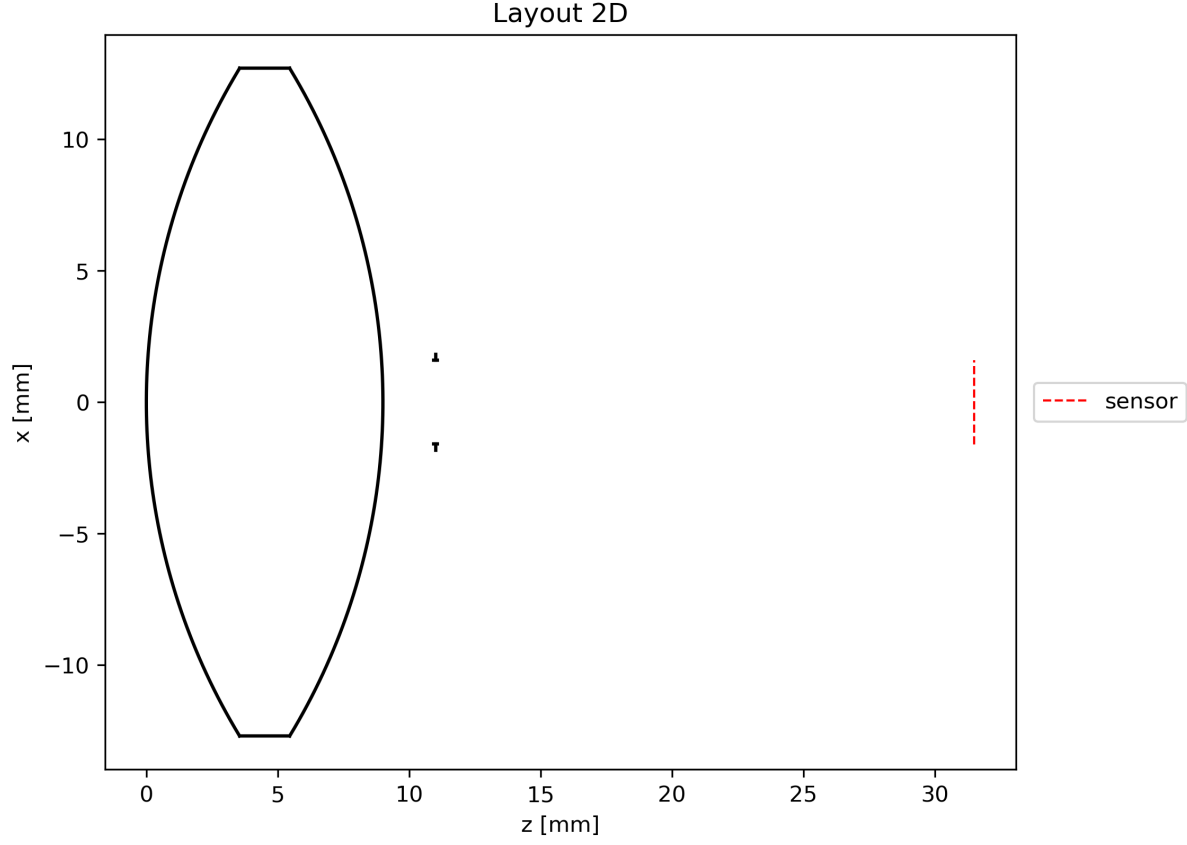
- Function test
- Layout & Ray visualization
- Best focus estimation
- Sampling number (N) sweep
- Wavelength ( $\lambda$ ) sweep
- Through-focus (D2) sweep
- Aperture sweep (OD)
- Off-axis sweep

Further, we consider a double-Gaussian lens US2532751A, and conducted:

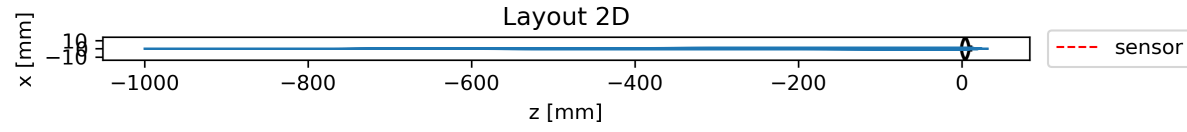
- Wavelength ( $\lambda$ ) sweep
- Off-axis sweep

### Function Test

Function tests are in `test_geo.py` and `test_ray_tracing.py`, mainly to verify the correctness of the geometric calculations and function implementations.



Lens layout.



Ray tracing.

### PSF Examples

After optimization, placing the sensor (mm) at the following distances *after the aperture* yields the best focus:

Table 1: Best focus distance vs. aperture

Aperture (mm)	1.6 (f/16)	3.175 (f/8)	6.35 (f/4)	12.7 (f/2)
Best Focus Distance (mm)	20.55	20.5	20.3	18.7

**Observation:** The best sensor-to-aperture distance varies slightly with aperture size, shifting from 20.55 mm at f/16 to 18.7 mm at f/2 due to increased spherical aberration at larger apertures.

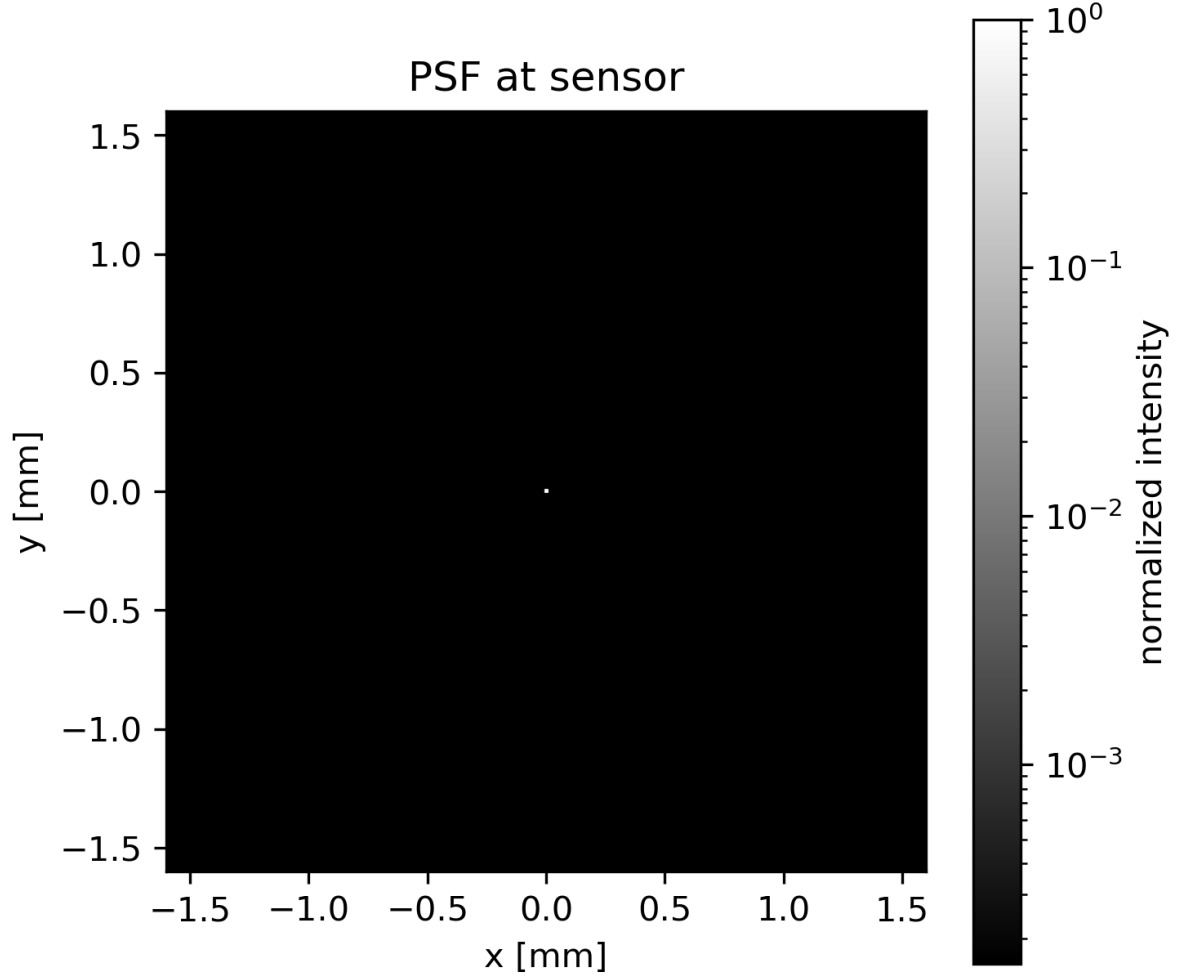


Figure 1: PSF (log scale) at best focus for **3.175 (f/8)** .

### N-sweep (sampling)

We swept  $N \in \{50, 100, 400, 1600, 3200, 6400\}$  and computed metrics vs.  $N$ . To probe focus sensitivity, we also used a larger aperture  $OD = 6.35$  mm  $D2 = 20.3$  mm and repeated the PSF analysis.

Illustrations for  $N = \{50, 400, 3200\}$  are shown below (more in the folder):

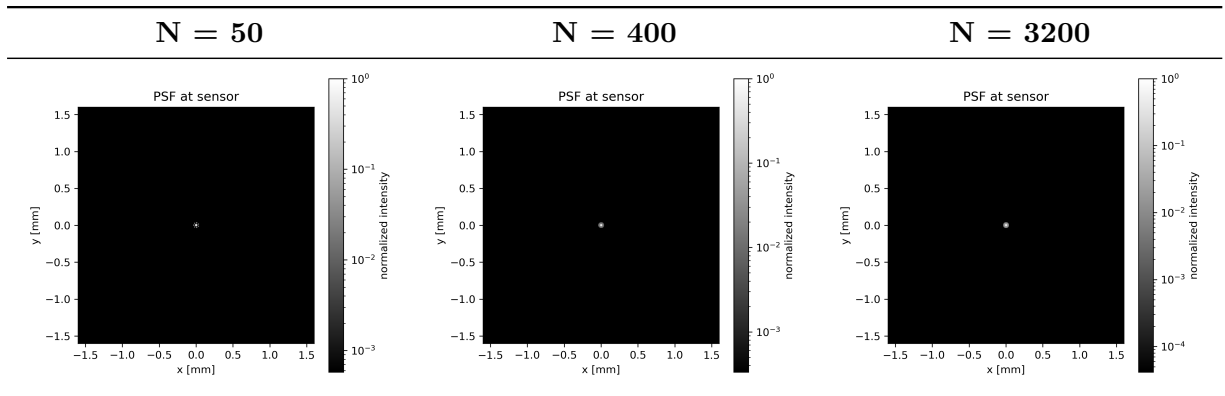


Table 2: PSF snapshots vs. sampling count  $N$ .

EE50 and RMS metrics are recorded in `metrics.csv` and plotted in:

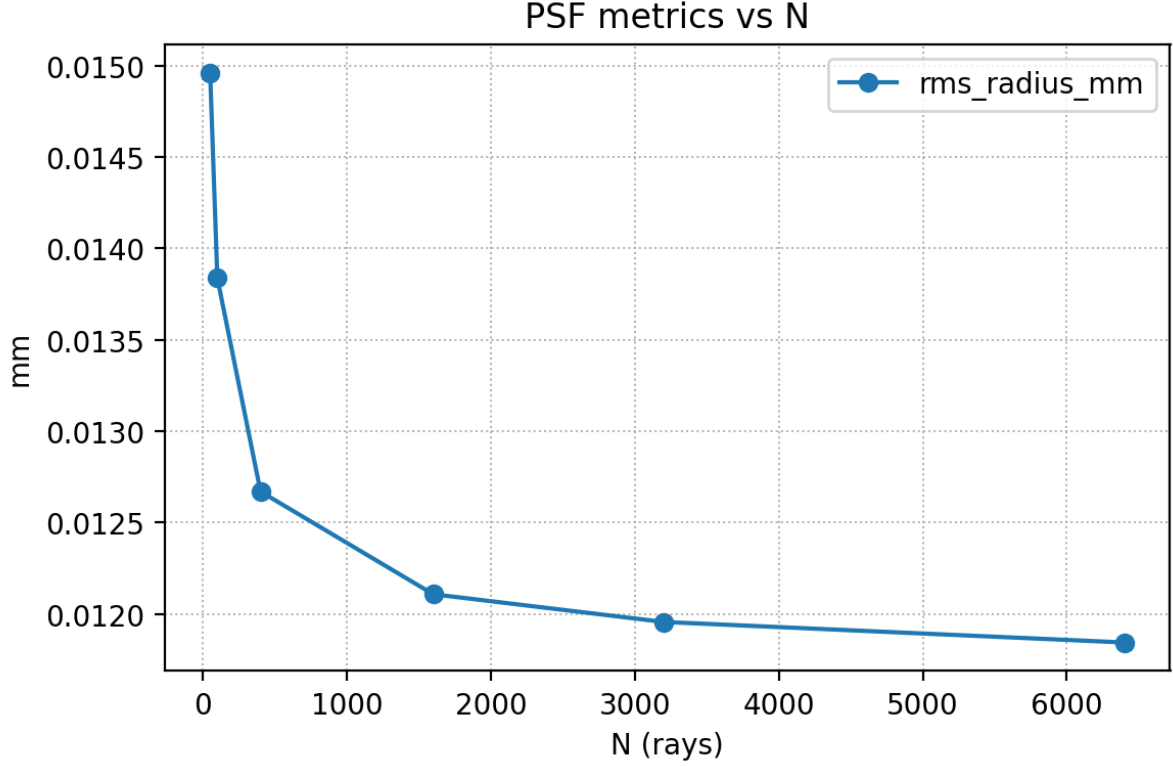


Figure 2: Metrics vs.  $N$ .

**Observation:** The convergence begins around  $N \geq 1600$ , where RMS values stabilize to  $\sim 0.045$  mm and  $\sim 0.021$  mm, indicating sufficient ray sampling density. We choose  $N = 3200$  for the remaining experiments.

### Wavelength Sweep

We sweep  $\lambda \in \{430, , 670\}$  nm,, with sweep\_step 10nm (within the visible range):

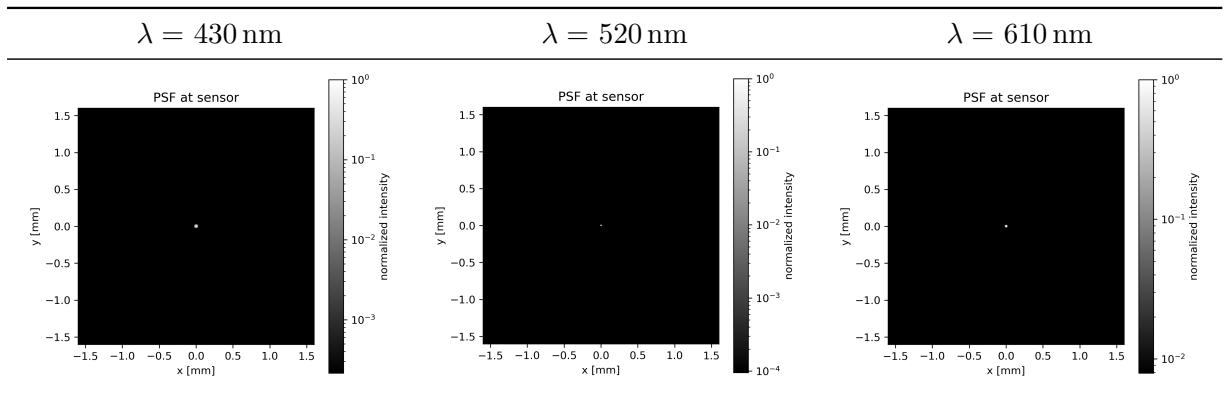


Table 3: PSF vs. wavelength.

Metrics are in `metrics.csv`; plot:

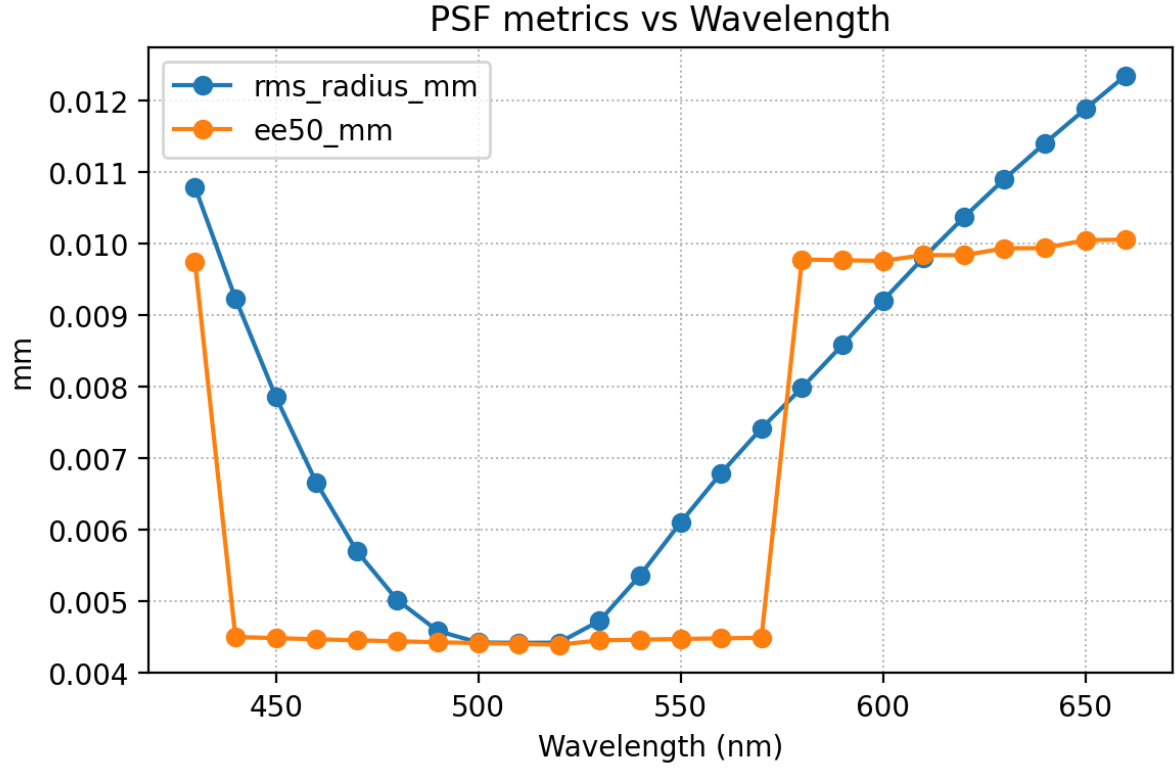


Figure 3: Metrics vs. wavelength.

**Observation:** With BK7 dispersion enabled, the smallest PSF occurs near  $\sim 500$  nm and grows toward both spectral ends (chromatic focus shift).

#### Through-focus (D2 sweep)

We sweep  $D_2 \in [19.5, 21.5]$  mm (sampling 13 steps). The best focus is at 20.5 mm.

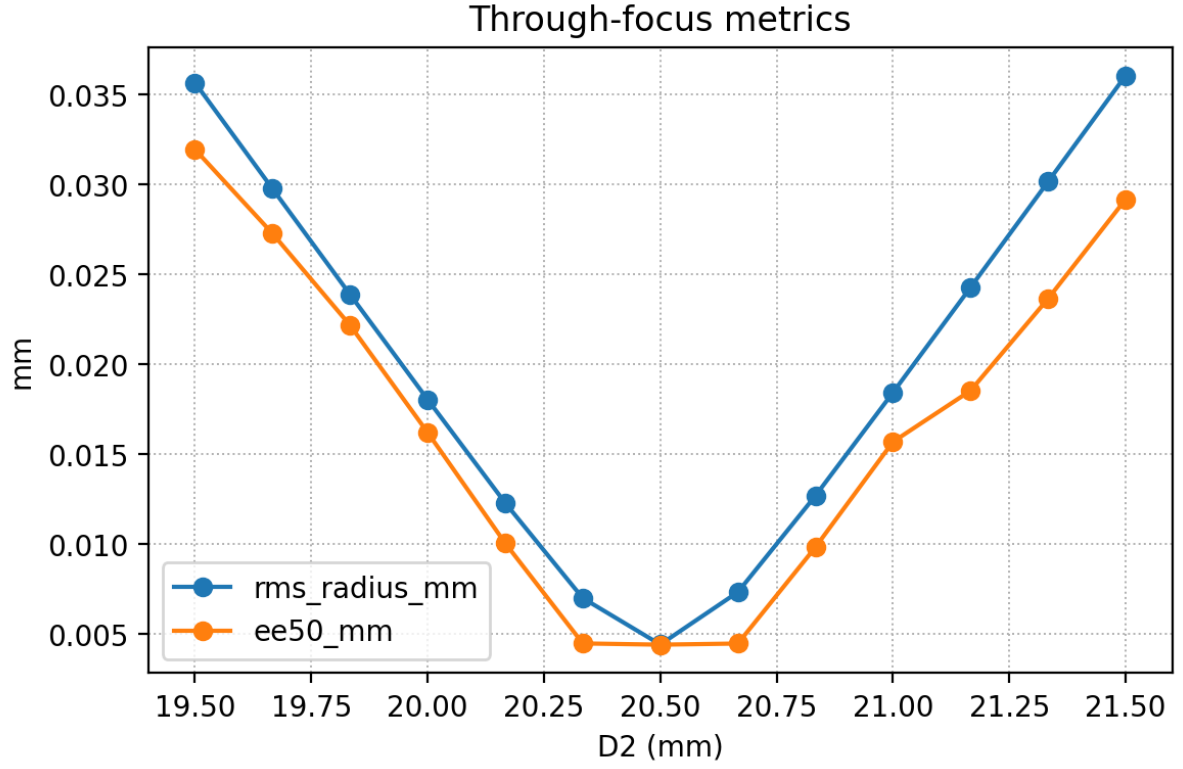


Figure 4: Metrics vs.  $D_2$  (through-focus sweep).

**Observation:** Moving away from 20.5 mm (e.g., toward 20.33 or 20.66) increases RMS and EE50 smoothly; the curve is slightly asymmetric due to real lens aberrations.

#### Aperture Sweep (OD)

We sweep  $\text{OD} \in \{1.5875 \text{ mm } (f/16), 3.175 \text{ mm } (f/8), 6.35 \text{ mm } (f/4), 12.7 \text{ mm } (f/2)\}$ .

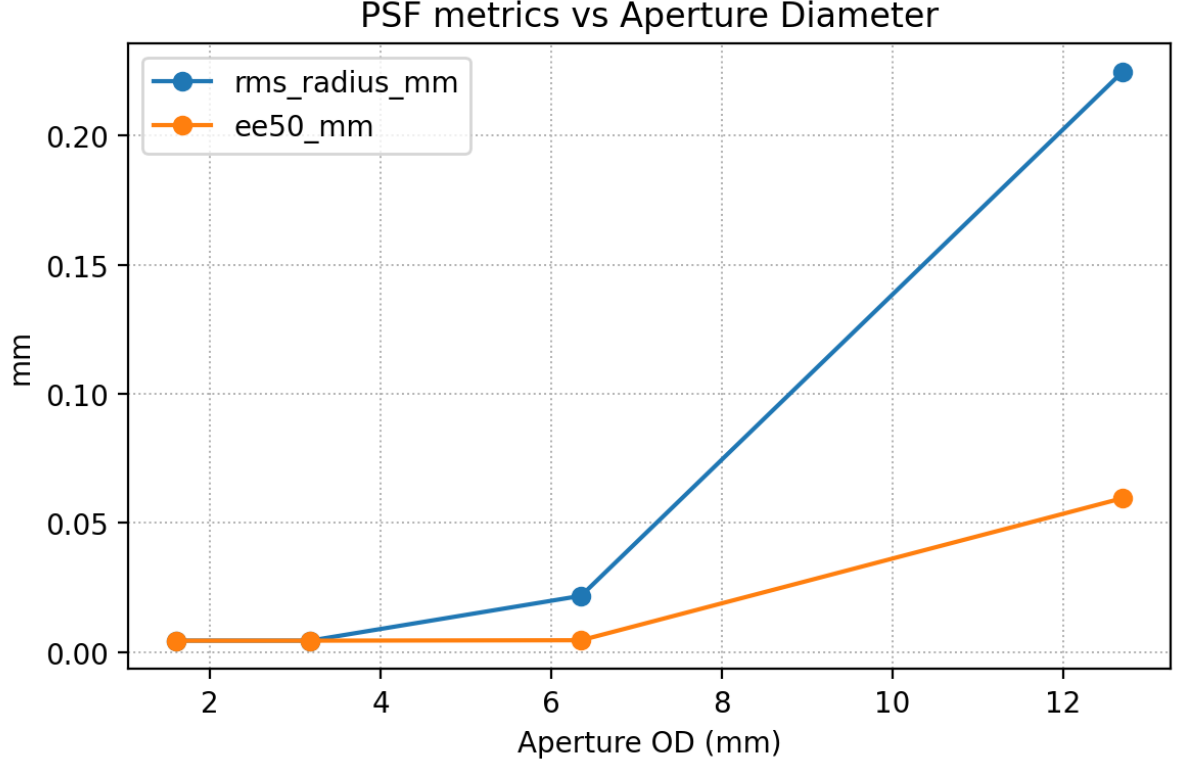


Figure 5: Metrics vs. aperture (OD).

**Observation:** As aperture increases from  $\sim 1.6$  to  $12.7$  mm, the PSF core (EE50) stays nearly constant at small-moderate apertures, while the halo (RMS) grows; at the largest aperture both EE50 and RMS increase noticeably. The sharpest results occur near smaller apertures ( $\sim 1.6$ – $3.2$  mm).

### Off-axis sweep

We consider  $OD = 6.35$  mm ( $f/4$ ),  $R2 = 20.3$  mm for better focus and field offsets  $-35, 35$  mm, sampling 36 steps:

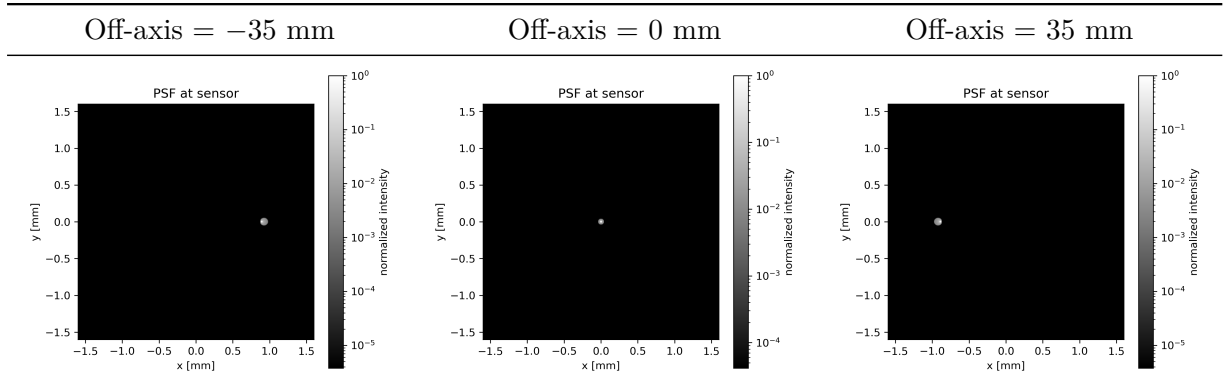


Table 4: PSF vs. field offset (biconvex).

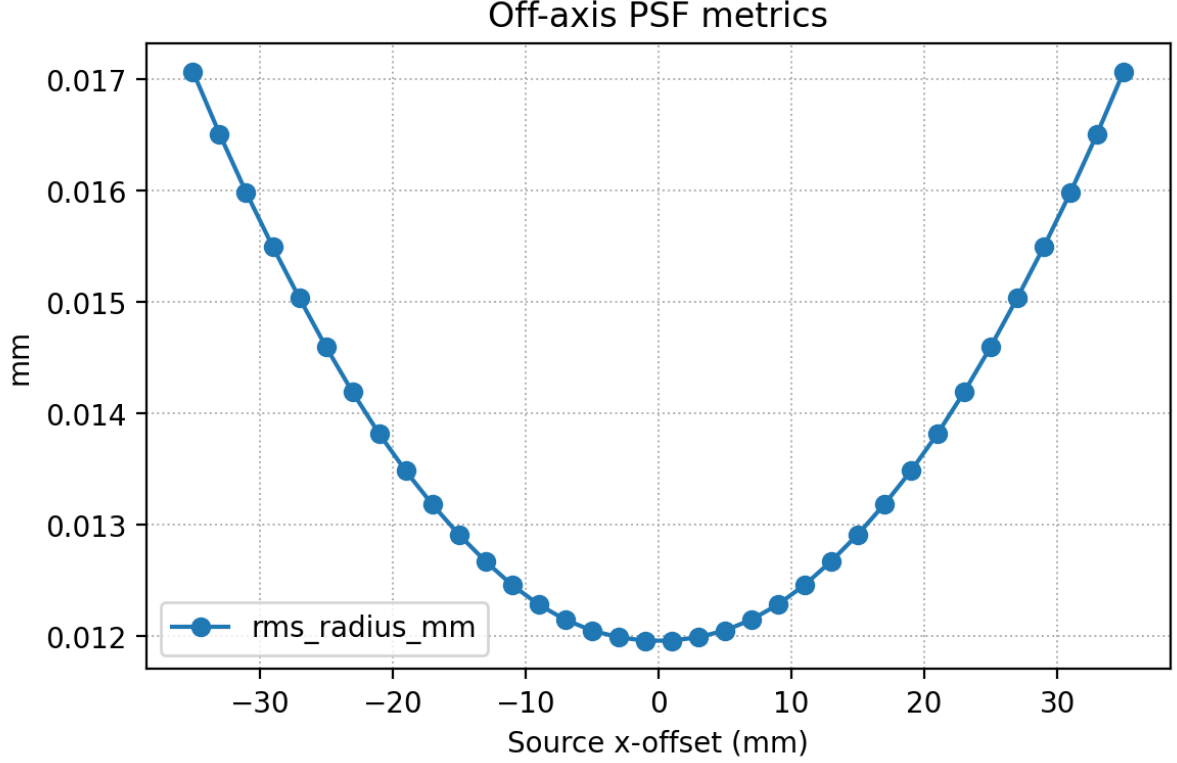


Figure 6: RMS vs. field offset.

**Observation:** As the source moves off-axis, the PSF centroid shifts roughly linearly with field; core size stays nearly constant for small offsets, with mild coma/asymmetry at larger field.

## 1.1 Discussion and Qualitative Analysis

### Sampling and Aliasing

With small  $N$ , the PSF shows speckle-like noise due to non-uniform pupil mapping; as  $N \gtrsim 1600$ , RMS and EE50 stabilize and the PSF becomes smooth. Mitigations: increase  $N$ ; average multiple seeds; sample uniformly on the pupil.

### Wavelength Dependence (Chromatic Aberration)

With BK7 dispersion,  $n(\lambda)$  decreases with  $\lambda$ ; effective focal length increases with  $\lambda$ . Thus a fixed sensor plane cannot be perfect for all wavelengths (blue focuses in front; red behind).

### Through-Focus Behavior

Sweeping  $D_2$  shows smooth degradation away from best focus (20.5 mm); curves are slightly asymmetric and steeper for larger apertures, matching expectations for residual spherical terms.

### Aperture Effect (f-number)

As OD increases from f/16 to f/2:

- EE50 remains nearly constant at small apertures;
- RMS grows at large apertures due to spherical aberration and coma.



## Off-Axis Source

Off-axis increases centroid shift and introduces coma at large field; best-focus distance varies mildly across field, indicating slight field curvature. A more complex lens group can suppress these effects (seen in the double gaussian lens experiment).

This indicates a trade-off between brightness and sharpness: smaller apertures ( $f/8$ – $f/16$ ) yield tighter PSFs and reduced aberrations, while very large apertures ( $f/2$ ) show blur halos and energy spread.

## 1.2 Algorithmic Correction of Aberrations

Aberrations (defocus, spherical, coma, astigmatism) broaden PSF and reduce contrast. Modeling as a spatially varying PSF  $h(x, y)$ , we compare classical vs. learning-based:

Table 5: Classical deconvolution vs. neural approaches

Aspect	Classical Deconvolution	Neural Network Approach
Principle	Linear inversion (e.g., Wiener, RL) with known PSF	Data-driven mapping from blurred to sharp
Pros	Interpretable; predictable; no training data	Handles complex/chromatic/field-dependent aberrations; flexible
Cons	Sensitive to noise/PSF mismatch; non-stationary PSF is hard	Needs data; potential overfitting
Best use	Mild blur, stationary PSF	Complex scenarios, data-rich pipelines

## 1.3 Model Refinement and Efficiency

**Physical accuracy:** include diffraction; model sensor pixel response (e.g., microlens/MTF); consider material tolerances (temperature).

**Computation:** vectorize intersections; enable GPU acceleration.

**Function:** extend to scene rendering.

## Conclusion

The simulator reproduces key behaviors of the Thorlabs LB1761 singlet and the Double-Gauss configuration. Major outcomes:

- **Functional:** PSF metrics (RMS, EE50); even-grid alignment fix; sampling functions by object distance; `build_lens()`; modular structure; unit tests.
- **Validated optics:** Correct Snell refraction and intersections; PSF metrics converge for  $N \geq 1600$ ; expected trends for wavelength, focus, aperture, and field.

## Extra (Double-Gaussian results)

We repeat wavelength and off-axis sweeps on a Double-Gauss (aperture  $\approx f/4$ ).

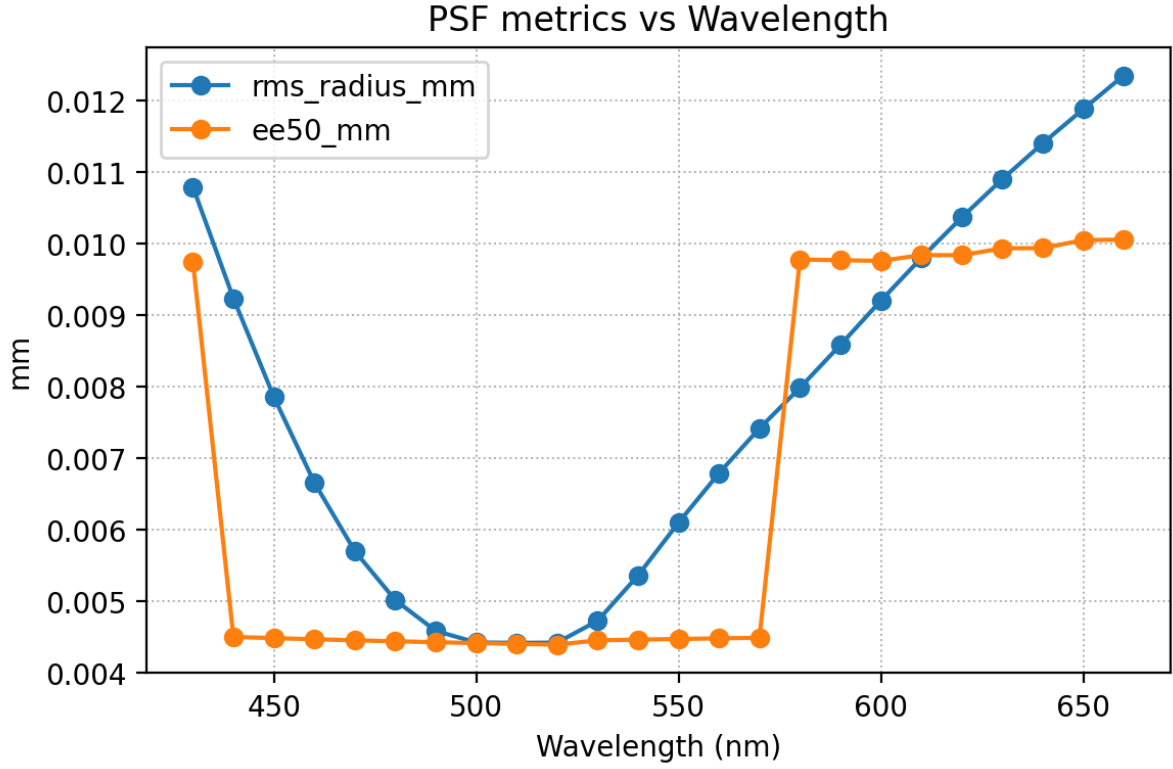


Figure 7: Double-Gauss: metrics vs. wavelength.

Wavelength sweep.

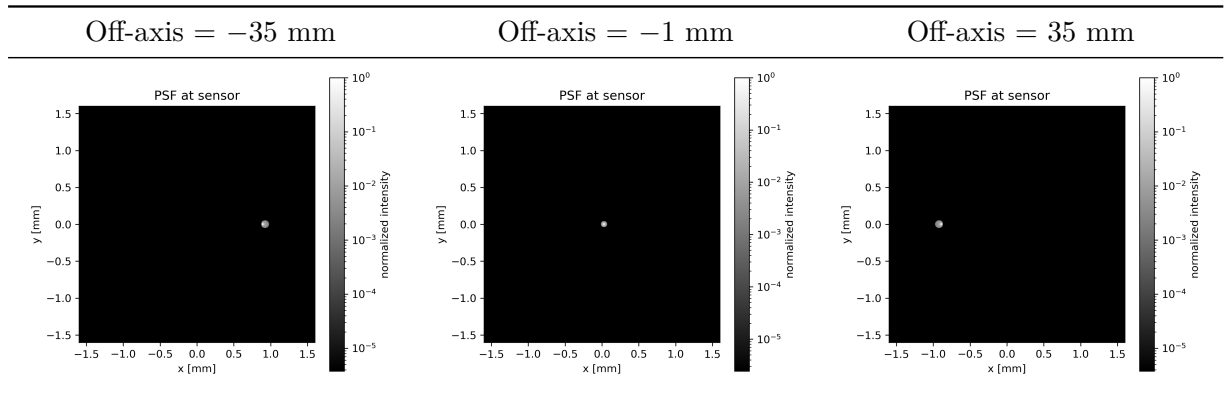


Table 6: PSF vs. field offset (Double-Gauss).

**Off-axis sweep. Observation:** With improved lens design, artifacts such as coma and other aberrations are significantly reduced, yielding better focus consistency across wavelengths—especially evident in the Double-Gauss design.